IET Microwaves, Antennas & Propagation

Research Article

IET Journals
The Institution of Engineering and Technology

Achieving uniform perpendicular magnetic field distribution for near-field ultra-high frequency radio-frequency identification

ISSN 1751-8725
Received on 5th June 2015
Revised on 21st August 2015
Accepted on 18th September 2015
doi: 10.1049/iet-map.2015.0368
www.ietdl.org

Laiwei Shen[1], *Wei Zhuang*[2,3] ✉, *Wanchun Tang*[2,3], *Jian Ma*[2,3]

[1]*Department of Communication Engineering, Nanjing University of Science and Technology, Nanjing, People's Republic of China*
[2]*Jiangsu Key Laboratory on Opto-electronic Technology, Nanjing Normal University, Nanjing, People's Republic of China*
[3]*Jiangsu Center for Collaborative Innovation in Geographical Information Resource Development and Application, Nanjing 210023, People's Republic of China*
✉ *E-mail: zhuangwei@njnu.edu.cn*

Abstract: In this study, a new antenna is proposed to achieve uniform perpendicular magnetic field distribution for near-field ultra-high frequency radio-frequency identification. The antenna is based on 'interdigital-oppositely directed currents (ODCs)' that is formed by introducing another current between the two oppositely directed currents of ODCs. By adjusting the feeding phase of the newly introduced current, the uniformity of perpendicular magnetic field distribution can be improved. The design procedure of the antenna is presented and the uniform perpendicular magnetic field distribution of the antenna is achieved and verified by experiments. When the transmitting power of the proposed antenna is 1 W, the interrogation area for 100% tag detection is 49×16 cm^2 with an observing height of 5 cm for Impinj J41 near-field tags.

1 Introduction

Recently, ultra-high frequency (UHF) near-field radio-frequency identification (RFID) has attracted a lot of academic attention for its great potential at the item level tracking and identifying. An UHF near-field RFID system is generally composed of reader, reader antenna and near-field tags. The reader antenna is designed to generate a perpendicular magnetic field near the antenna. Tags are usually designed as small loop antennas so that the power can be transferred from the reader antenna through inductive coupling. The tag can only be read successfully when the induced voltage on the tag chip is bigger than the threshold voltage. With rough calculation, for most commercial near-field tags, the magnetic field normal to the surface of the tag should be >-20 dBA/m [1–3], and the value will be further reduced with the improvement of reading sensitivity of tag chips.

UHF near-field RFID proves to be of great potential in item level identification for its advantage in reading stability, compared with conventional far-field RFID. The biggest challenge in UHF near-field RFID application, however, is the generation of a uniform perpendicular magnetic field ($|H_z|$) near the antenna to ensure stable identification in a large interrogation area since tags are generally placed parallel to the reader antenna.

There are several methods to realise uniform $|H_z|$ distribution [3–11]. The first method is keeping the current along a loop antenna in-phase by dividing the solid loop into individually resonant segments [4–6]. This concept was first presented by Dobkin *et al.* in [4], where a circular loop is divided into several segments, with each segment composed of a metal line and a lumped capacitance in series. Chen *et al.* [5, 6] also proposed a broadband segmented loop antenna by employing zero-phase-shift line, in which distributed capacitances are used instead of lumped capacitances.

The second method is using dipoles to form an electrically large loop with in-phase current [7–9]. In [7], four dipoles are placed end to end to form a closed square loop, and fed by the currents with the same phases after careful design. Both of the above mentioned two methods can be used to achieve a relatively large and uniform $|H_z|$ distribution, and hence to enlarge the interrogation area. However, the structures of the antennas are complex and the area is hard to be further expanded.

A novel printed-folded dipole antenna with a simple structure was proposed in [10]. The antenna is designed based on the phenomenon that two closely spaced oppositely directed currents (ODCs) can generate a strong magnetic near-field between them [3, 11]. Unfortunately, the $|H_z|$ right above the current almost declines to a value smaller than -20 dBA/m so that the tag can hardly be read at present. This will cause inconvenience in some applications. To solve this problem, Balanis [12] proposed a new structure (called 'interdigital-ODCs' in this paper) which is formed by introducing another current between the two currents of the ODCs, to achieve a uniform $|H_z|$ distribution. By adjusting the feeding phases of the currents of the 'interdigital-ODCs', the uniformity of $|H_z|$ distribution can be improved with $|H_z| > -20$ dBA/m right above the currents. However, the theoretic analysis and then the design guideline are not given in [12].

In this paper, therefore, we will analyse the 'interdigital-ODCs' in detail in Section 2 and present the design guideline of the 'interdigital-ODC'-based antenna in Section 3. Sections 4 and 5 give the experimental results and conclusions, respectively.

2 'Interdigital-ODCs' for uniform perpendicular magnetic field distribution

To study the characteristics of the 'interdigital-ODCs', let us first examine the $|H_z|$ distribution of the ODCs. As shown in Fig. 1, an ODC-based antenna is designed with four arms and side feed at the right side, a little different from that of [10]. a is about half wavelength long and chosen as 12.5 cm in this paper at the resonant frequency 920 MHz, so that the currents on the adjacent 'arms' are in opposite direction, forming three pairs of ODCs in total. Other geometric parameters are given in Fig. 1.

2.1 $|H_z|$ distribution of the ODCs

To examine the $|H_z|$ distribution of the ODCs, let us consider the perpendicular magnetic field (referred as $|H_z|$ in this paper) distribution of the ODCs at first. For simplicity, assume that the direct currents are carried on the ODCs but in opposite directions,

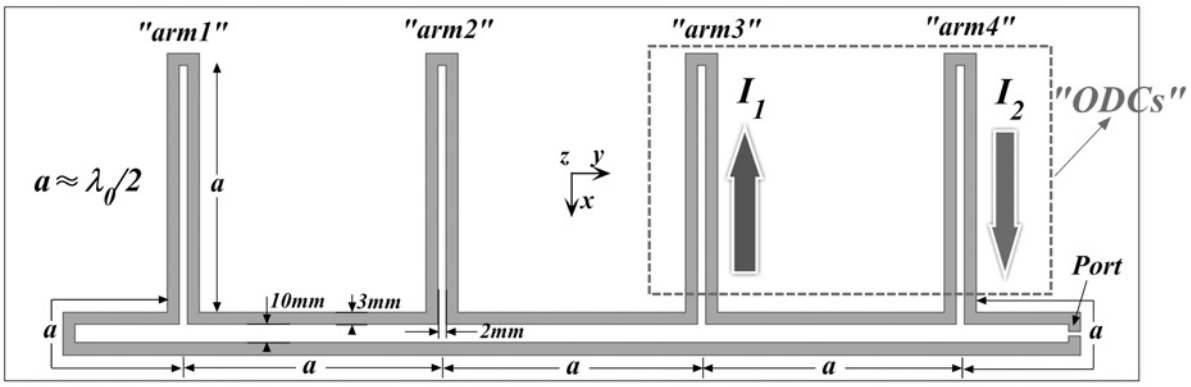

Fig. 1 *Configuration of the ODC-based antenna*

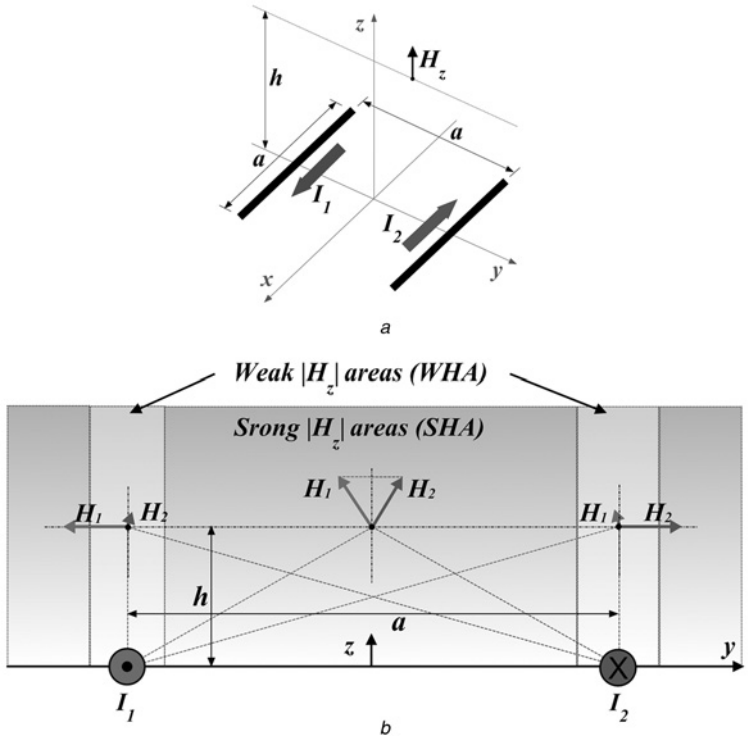

Fig. 2 *ODCs [3, 10]*

a Structure of the ODCs
b WHA and SHA of the ODCs

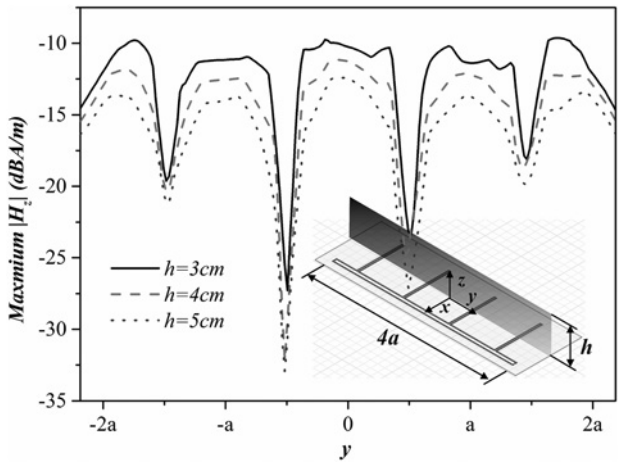

Fig. 3 *Simulated $|H_z|$ distribution of the ODC-based antenna along the y-axis for different heights (h) at 920 MHz with a = 12.5 cm*

as shown in Fig. 2*a*. One can see that the $|H_z|$ is large in the region between the ODCs, which is denoted as 'strong $|H_z|$ area (SHA)' in this paper. However, in the region right above the ODCs, the $|H_z|$ is very small compared with the horizontal magnetic field (see Fig. 2*b*), and therefore this region is denoted as 'weak $|H_z|$ area (WHA)' in this paper.

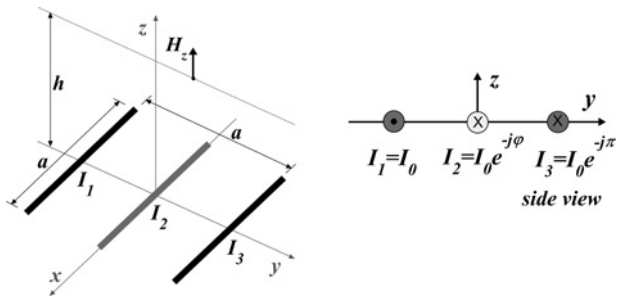

Fig. 4 *Proposed 'interdigital-ODCs'*

IET Microw. Antennas Propag., 2016, Vol. 10, Iss. 2, pp. 215–222

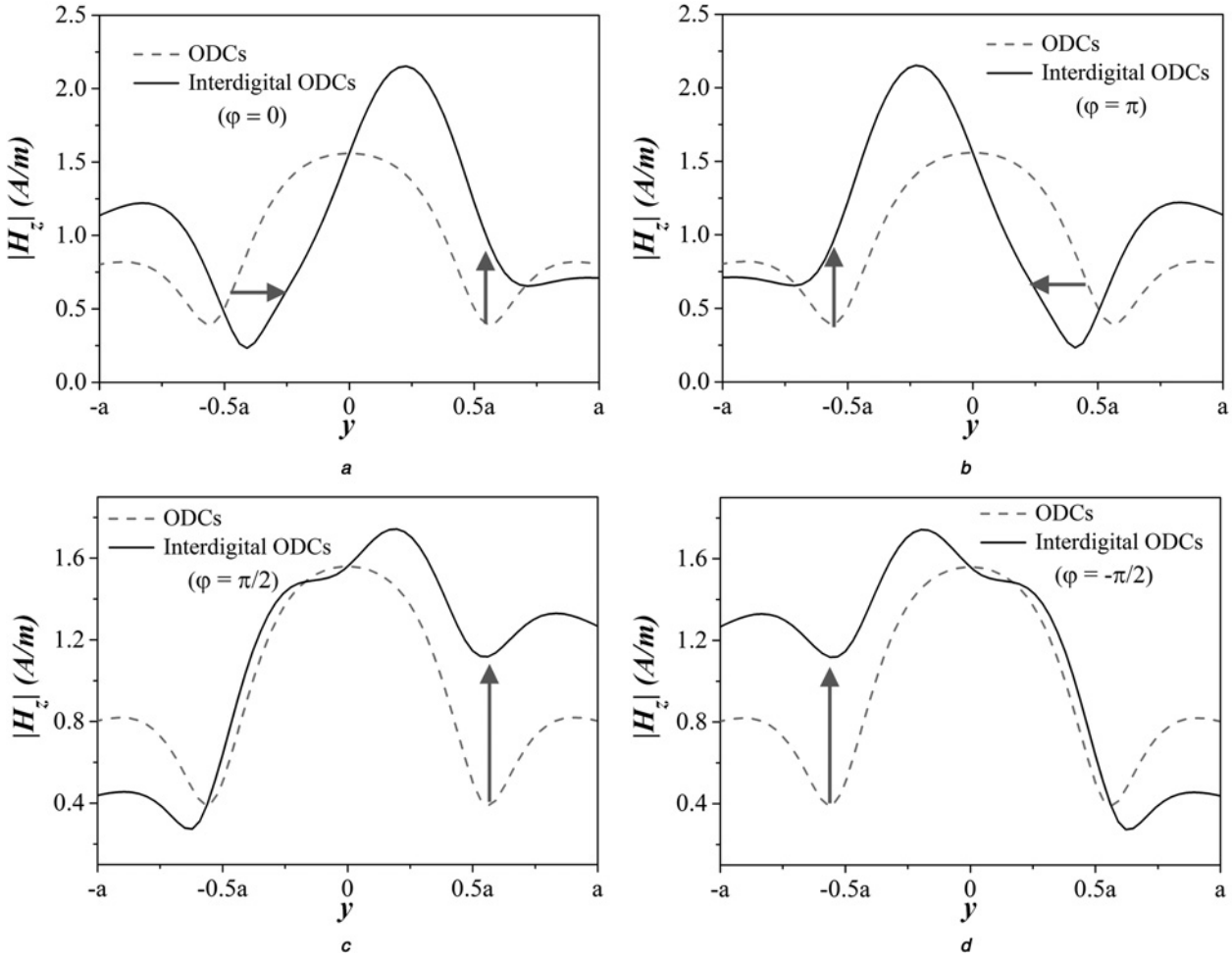

Fig. 5 *$|H_z|$ distribution of proposed 'interdigital-ODCs' along the y-axis with different φ (the phase of I2) at 920 MHz with an observing height of 5 and a = 12.5 cm*

If alternative currents are carried on ODCs, the SHA and WHA always exist and can be verified by the following simulations. The $|H_z|$ distribution of the antenna in Fig. 1 for different height h is studied in high frequency structure simulator (HFSS), with the input power of 1 W and frequency of 920 MHz. As shown in Fig. 3, the SHAs and WHAs are always present and distributed alternately along the y-axis no matter which value the h is. It means that the $|H_z|$ distribution is not uniform, which will cause inconveniences such as missed detection in many item level applications of near-field RFID.

2.2 $|H_z|$ distribution of 'interdigital-ODCs'

To make the $|H_z|$ distribution of the ODCs uniform, one more current is added in between the two currents of the ODCs, to form the so-called 'interdigital-ODCs' as shown in Fig. 4. The $|H_z|$ produced by this newly added current I_2 is expected to compensate that in the WHAs right above the currents I_1 and I_3 of the ODCs. However, the phase of I_2 will have an important effect on the compensation.

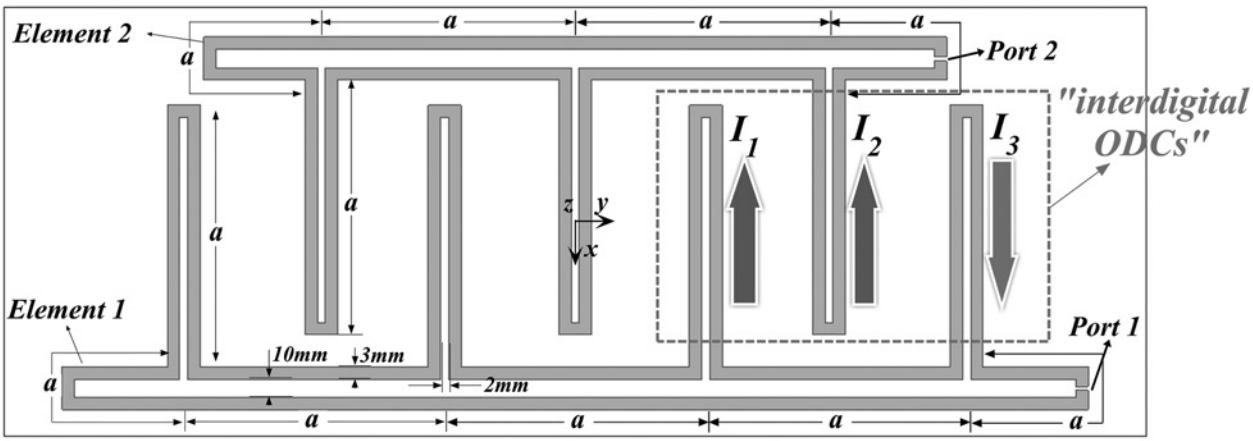

Fig. 6 *Configuration of the 'interdigital-ODC'-based antenna without feeding network, a = 12.5 cm*

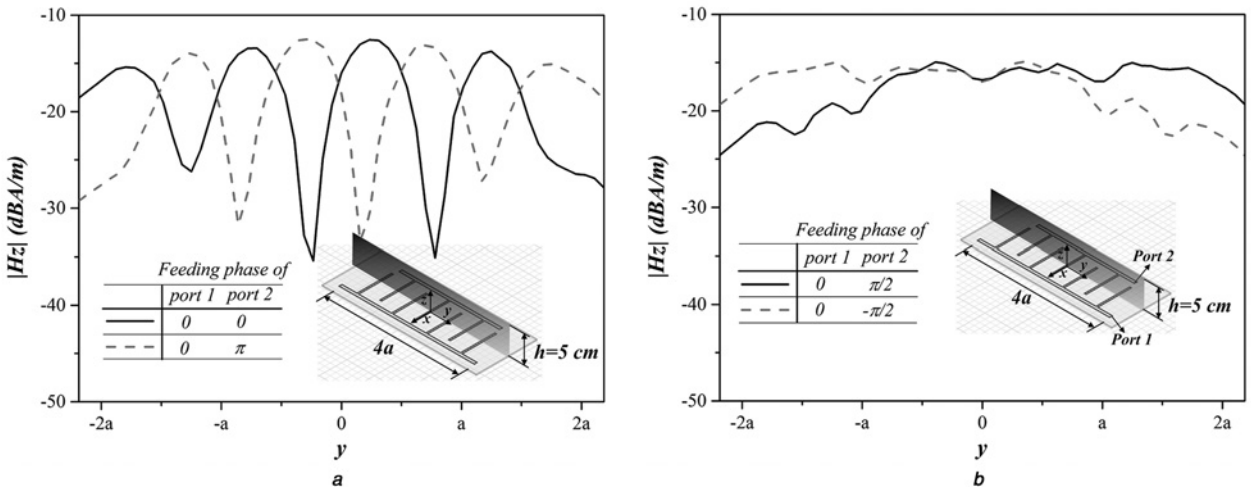

Fig. 7 *Simulated $|H_z|$ distribution of the 'interdigital-ODC'-based antenna with different phase of feeding current at port 2*

a Phase of feeding current at port 2 equals to 0 and π
b Phase of feeding current at port 2 equals to $\pi/2$ and $-\pi/2$ operating frequency is 920 MHz and $a = 12.5$ cm

Assume that the magnitude of all the three currents (I_1 to I_3) is I_0, while the phases are 0, φ and π, respectively. According to [13], the total $|H_z|$ distribution along the y-axis at height h can be written as follows:

$$\begin{aligned}|H_z| &= |H_{z1} + H_{z2} + H_{z3}| \\ &= |I_0 f_1(y) + I_0 \mathrm{e}^{-\mathrm{j}\varphi} f_2(y) + I_0 \mathrm{e}^{-\mathrm{j}\pi} f_3(y)|,\end{aligned} \tag{1}$$

where

$$f_1(y) = -\frac{(y + a/2)}{4\pi {r_1}^2 \mathrm{j}}\left[2\mathrm{e}^{-\mathrm{j}kR_1} - 2\cos\left(\frac{ka}{2}\right)\mathrm{e}^{-\mathrm{j}kr_1}\right],$$

$$f_2(y) = -\frac{y}{4\pi {r_2}^2 \mathrm{j}}\left[2\mathrm{e}^{-\mathrm{j}kR_2} - 2\cos\left(\frac{ka}{2}\right)\mathrm{e}^{-\mathrm{j}kr_2}\right],$$

$$f_3(y) = -\frac{(y - a/2)}{4\pi {r_3}^2 \mathrm{j}}\left[2\mathrm{e}^{-\mathrm{j}kR_3} - 2\cos\left(\frac{ka}{2}\right)\mathrm{e}^{-\mathrm{j}kr_3}\right],$$

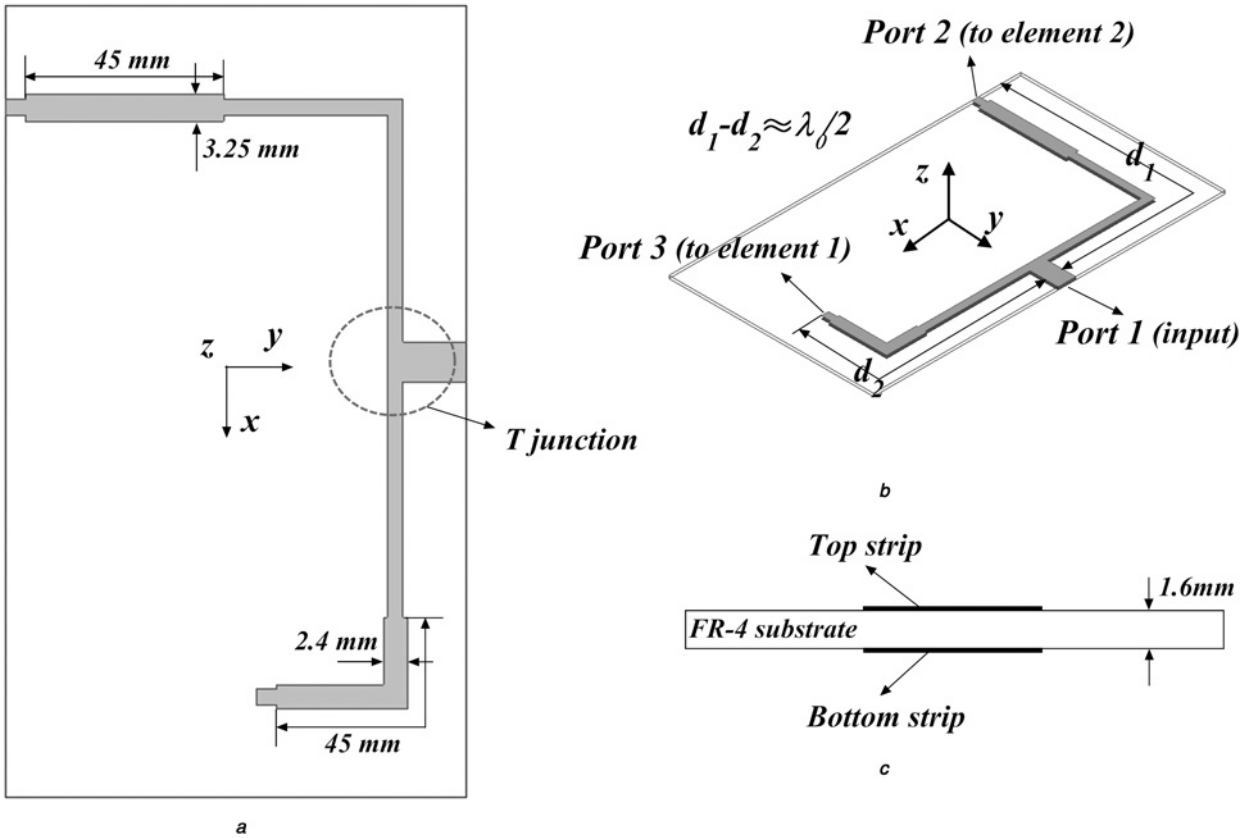

Fig. 8 *Configuration of the feeding network*

a Top view
b Perspective view
c Side view

IET Microw. Antennas Propag., 2016, Vol. 10, Iss. 2, pp. 215–222

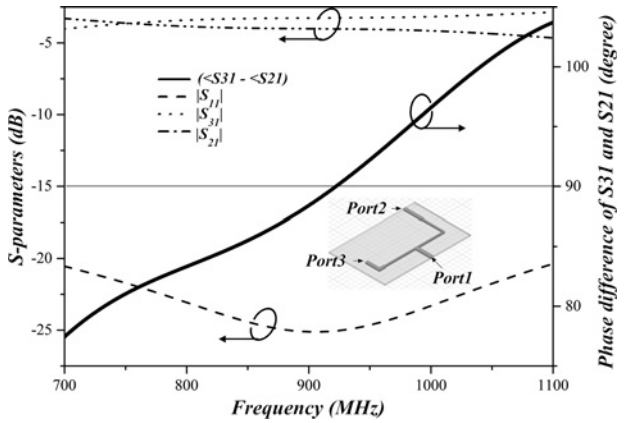

Fig. 9 *Simulated S-parameters of the feeding network*

and

$$r_1 = \sqrt{\left(y + \frac{a}{2}\right)^2 + h^2}, \quad r_2 = \sqrt{y^2 + h^2}, \quad r_3 = \sqrt{\left(y - \frac{a}{2}\right)^2 + h^2},$$
$$R_1 = \sqrt{\left(\frac{a}{2}\right)^2 + r_1^2}, \quad R_2 = \sqrt{\left(\frac{a}{2}\right)^2 + r_2^2}, \quad R_3 = \sqrt{\left(\frac{a}{2}\right)^2 + r_3^2}. \tag{2}$$

with

$$k = \omega\sqrt{\mu\varepsilon}.$$

The $|H_z|$ distribution of the 'interdigital-ODCs' can be obtained by (1) and (2) for different φ (phase of current I_2), and the results are shown in Figs. 5*a–d*. For comparison, the $|H_z|$ distribution of the ODCs is also added in dashed lines. When $\varphi = 0$, Fig. 5*a* shows that the $|H_z|$ in the region of WHA right above current I_3 increases a little (from about 0.4 to 0.7 A/m), while the WHA right above current I_1 moves towards current I_2. If $\varphi = \pi$, the opposite trend will be obtained, as shown in Fig. 5*b*. The implication is that the compensation of the $|H_z|$ in the region of WHAs is not effective when the phase φ of current I_2 is 0 or π.

However, if $\varphi = \pi/2$ as shown in Fig. 5*c*, the $|H_z|$ in the region of WHA right above current I_3 increases from about 0.4 to 1.2 A/m, while the WHA right above current I_1 still exists. This means the uniformity of the $|H_z|$ distribution can be improved. Opposite trend can also be obtained and shown in Fig. 5*d* if $\varphi = -\pi/2$.

3 Antenna configuration and optimisation

3.1 Realisation of the 'interdigital-ODCs'

On the basis of the analysis of the 'interdigital-ODCs' in the previous section, two ODC-based antennas (elements 1 and 2) are combined interdigitally to form an 'interdigital-ODC'-based antenna as shown in Fig. 6, where element 1 is in fact the ODC-based antenna in Fig. 1. As can be seen, the WHAs of element 1 and the SHAs of element 2 are overlapped, and vice versa.

By setting the feeding phase φ of port 2 in Fig. 6 in the software HFSS, the $|H_z|$ distribution can be obtained and is shown in Fig. 7. From Fig. 7*a*, one can see that the WHAs appear periodically along the y-axis when φ is equal to 0 or π. However, if φ is equal to $\pm\pi/2$, the $|H_z|$ distribution shown in Fig. 7*b* is almost uniform although the curve experiences a slight incline.

3.2 Design of the feeding network

From the above analysis, $\pm\pi/2$ phase difference is preferred to achieve an uniform $|H_z|$ distribution. A feeding network similar

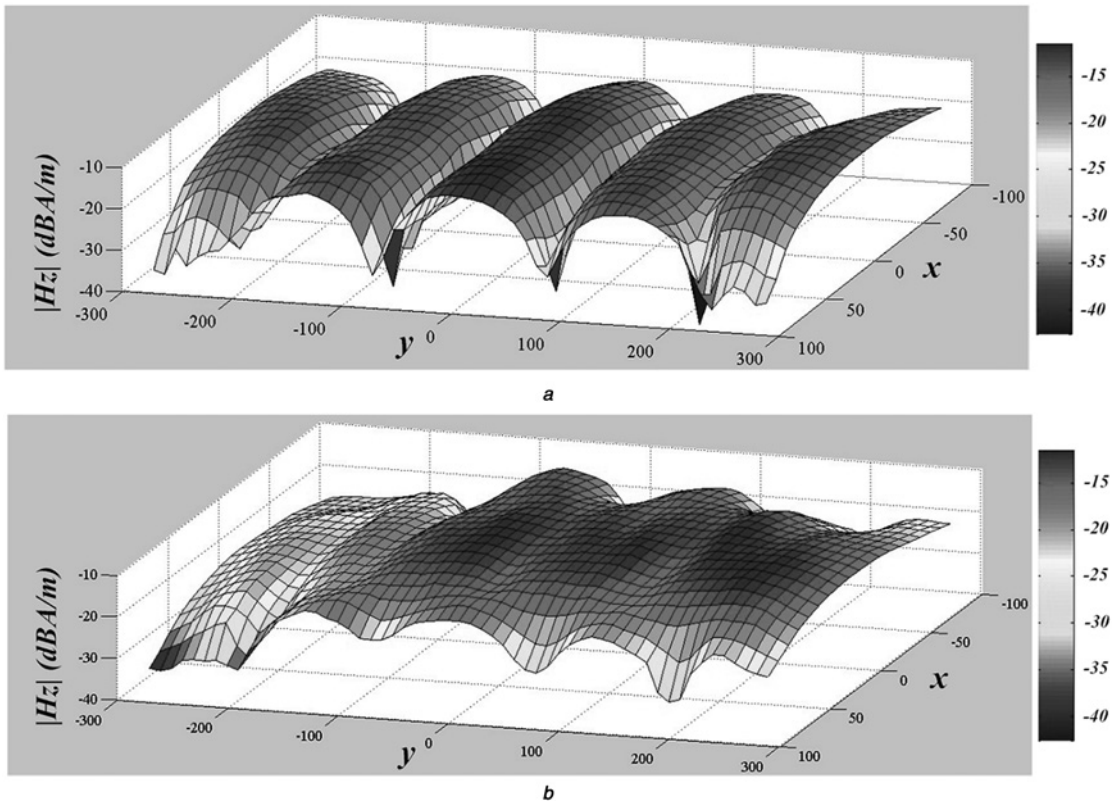

Fig. 10 *Simulated $|H_z|$ distributions with the input power 1 W at observing height 5 cm*

a ODC-based antenna
b Interdigital-ODC'-based antenna

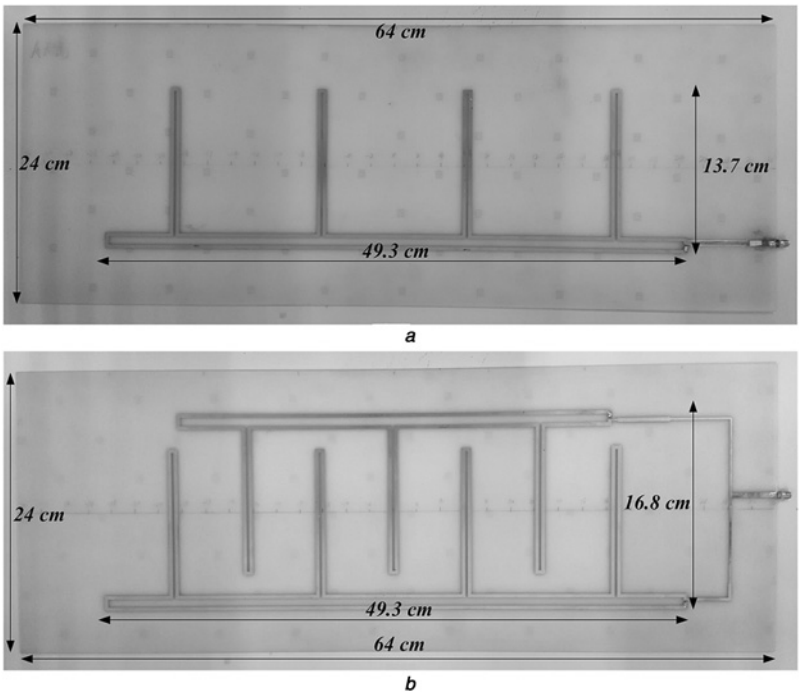

Fig. 11 *Fabricated antennas*
a ODC-based antenna
b 'Interdigital-ODCs-based antenna

to the feeding network of circular polarised antennas is designed to achieve $\pm\pi/2$ phase difference. The configuration of the feeding network is depicted in Fig. 8. A T junction of double-sided parallel-strip line is used to equally divide the input power, and $\pm\pi/2$ phase difference is achieved by lengthen one parallel-strip line with quarter wavelength. Another two quarter wavelength parallel-strip lines at ports 2 and 3 are used for impedance match. The simulated *S*-parameters by HFSS of the feeding network are given in Fig. 9, and $\pi/2$ phase difference is achieved at 920 MHz.

4 Results and discussion

4.1 Fabrication of the antenna

By connecting the feeding network of Fig. 8 to the 'interdigital-ODC'-based antenna in Fig. 6, the whole antenna is

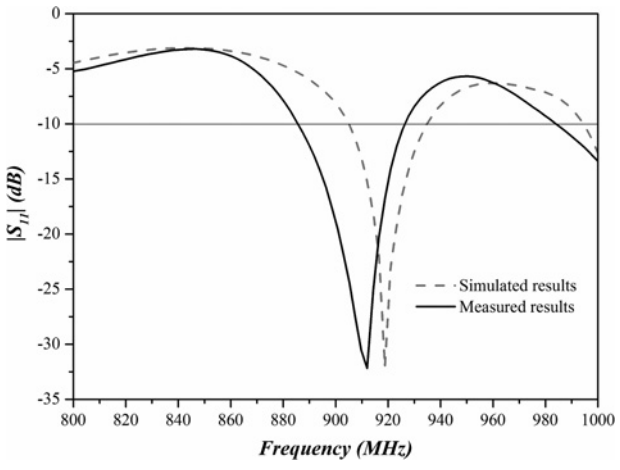

Fig. 12 *Simulated and measured return loss of the 'interdigital-ODC'-based antenna*

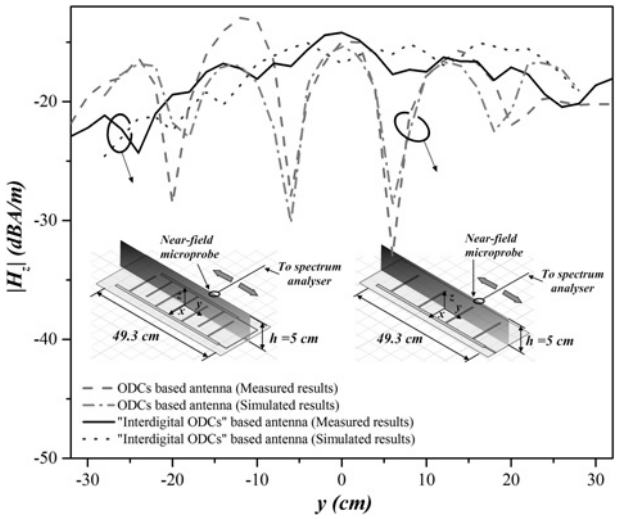

Fig. 13 *Measured $|H_z|$ along the y-axis at 5 cm height with simulated results for comparison*

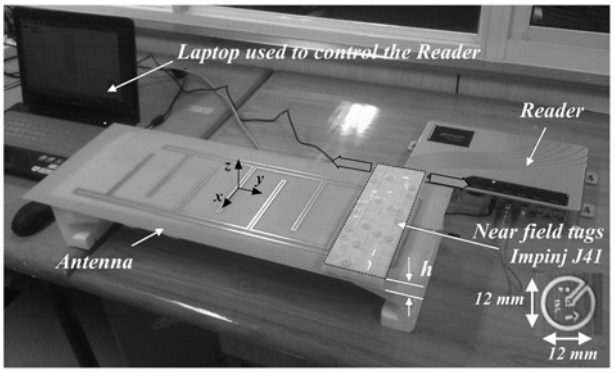

Fig. 14 *Photograph of the test setup*

IET Microw. Antennas Propag., 2016, Vol. 10, Iss. 2, pp. 215–222

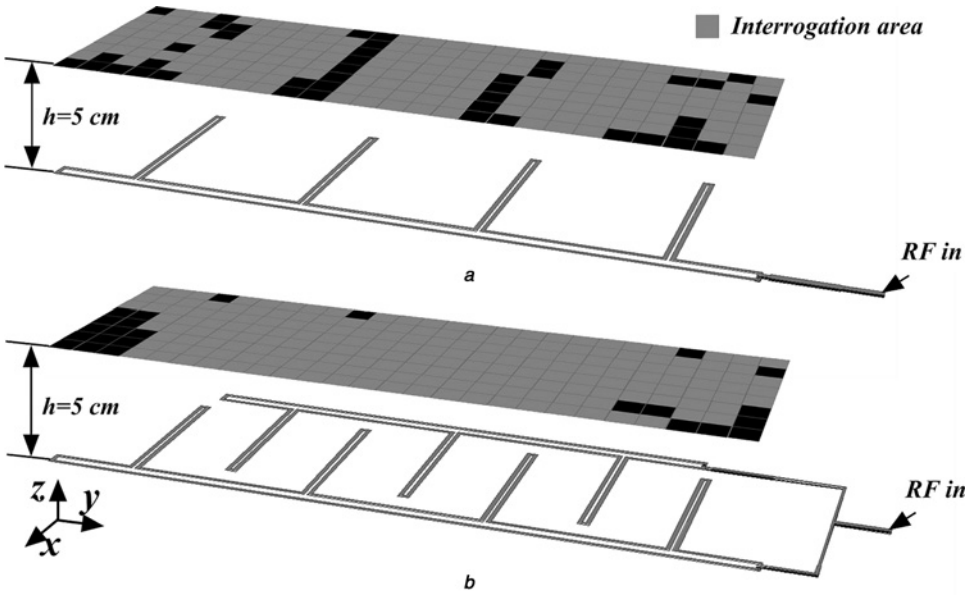

Fig. 15 *Measured interrogation area at the observing height 5 cm with 1 W input power*

a ODC-based antenna
b Interdigital-ODC'-based antenna

formed. Moreover, its corresponding $|H_z|$ distribution is simulated and is given in Fig. 10*b*. For comparison, the $|H_z|$ distribution of the ODC-based antenna in Fig. 1 is plotted in Fig. 10*a*. As can be seen, there are four obvious WHAs distributed above the four 'arms' of the ODC-based antenna, while the $|H_z|$ distribution of the 'interdigital-ODC'-based antenna is almost uniform.

Such an 'interdigital-ODC'-based antenna is fabricated on an FR-4 board with 1.6 mm in thickness and 4.4 in dielectric constant. The ODC-based antenna in Fig. 2 is also fabricated for comparison. As shown in Fig. 11, the 'interdigital-ODC'-based antenna occupies an area of 49.3×16.8 cm^2, while the ODC-based antenna occupies 49.3×13.7 cm^2.

4.2 Reflection coefficient and $|H_z|$ distribution of the antenna

Fig. 12 shows the measured reflection coefficient of the 'interdigital-ODC'-based antenna by vector network analyser (Agilent 8722ES), together with the simulated results for comparison. The measured resonant frequency is slightly shifted by 10 MHz compared with the simulated resonant frequency due to the fabrication error. The measured bandwidth ($|S_{11}| < -10$ dB) of the 'interdigital-ODCs' is about 40 MHz (887–927 MHz), which can completely cover the standard UHF band (920–925 MHz) in China.

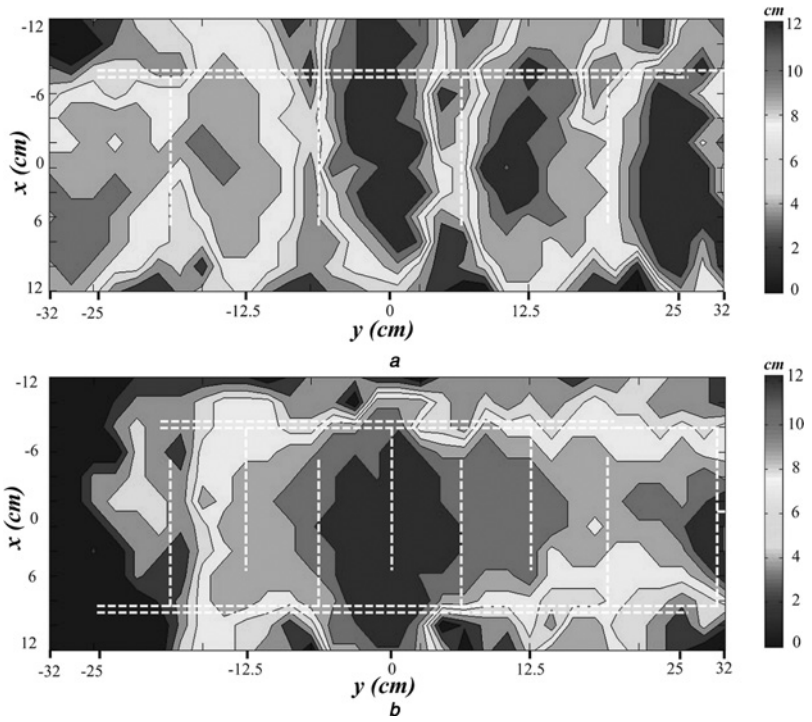

Fig. 16 *Measured reading distance (different colours for different reading distance)*

a ODC-based antenna
b 'Interdigital-ODC'-based antenna

The $|H_z|$ distributions of the fabricated antennas are measured using a near-field magnetic probe (Langer EMV Technik ICR HH 150–27) and a spectrum analyser (Agilent MXA N9020A). Fig. 13 shows that the measured $|H_z|$ along the y-axis at observing height of 5 cm, together with the simulations. As can be seen, $|H_z|$ distribution of the 'interdigital-ODC'-based antenna is relatively uniform and $|H_z|$ is bigger than −20 dBA/m from $y = -22$ to 27 cm at observing height of 5 cm. However, the $|H_z|$ of the ODC-based antenna is smaller than −20dBA/m when $y = -19$, −6, 6, 19 cm, exactly the positions right above the four 'arms'.

4.3 Interrogation area and reading distance of the antenna

To evaluate the interrogation areas of the antennas, Fig. 14 displays the test setup. The communication signal in UHF band is fed into the antenna by a commercial RFID reader (Marktrace RFID UHF Four Channel Fixed Reader MR6134E), and the laptop is utilised to control the reader. Forty-eight near-field tags are pasted on a 24×8 cm^2 foam board, where each tag occupies 2×2 cm^2. Since the area of the FR-4 board is 64×24 cm^2, eight measurements are needed to evaluate the interrogation area over the whole FR-4 board, by moving the foam board from right to left or vice versa. The tags are coded according to their positions so that the interrogation area is plotted according to the reading result of each tag. The near-field tag used in the experiment is Impinj J41, which meets standard ISO 18000-6C, EPC Class1 Gen2.

Fig. 15 shows the measured interrogation area of the proposed 'interdigital-ODC'-based antenna and the ODC-based antenna at observing height of 5 cm. The test results show good agreement with the simulated $|H_z|$ distribution in Fig. 10. As can be seen, the interrogation area of the 'interdigital-ODC'-based antenna for 100% tag detection is 49×16 cm^2 at an observing height of 5 cm, while the interrogation area of the ODC-based antenna is divided into five parts by four WHAs and the tags cannot be read in the regions right above the ODCs.

The measured reading distance of the ODC-based antenna and the 'interdigital-ODC'-based antenna are shown in Figs. 16*a* and *b*, respectively. The maximum reading distance of the 'interdigital-ODC'-based antenna is 14 cm, which is comparable with the maximum reading distance of the ODC-based antenna (15 cm).

5 Conclusion

In this paper, the 'interdigital-ODCs' is proposed for the compensation of the weak $|H_z|$ areas of ODCs to achieve a uniform magnetic field distribution for a large stable interrogation area. The concept of 'interdigital-ODCs' is realised with two ODC-based elements and a feeding network to produce phase difference. Such an 'interdigital-ODC'-based antenna is designed and fabricated on an FR-4 board, and the simulations agree well with the experiments. When the transmitting power of the proposed antenna is 1 W, the interrogation area for 100% tag detection is 49×16 cm^2 with an observing height of 5 cm for Impinj J41 near-field tags.

6 Acknowledgments

This work was supported by the Fundamental Research Funds for the Central Universities NJ20150019, and the Natural Science Fund for Colleges and Universities in Jiangsu Province (15KJB510017), and the Priority Academic Program Development of Jiangsu Higher Education Institutions (PAPD) at Nanjing Normal University.

7 References

1 'Monza 2'. Available at http://www.impinj.com/products/tag-chips/
2 'Higgs 2'. Available at http://www.alientechnology.com/tags/rfid_ic.php
3 Cho, C., Ryoo, J., Park, I., *et al.*: 'Design of a novel ultra-high frequency radio-frequency identification reader antenna for near-field communication using opposite directed currents', *IET Microw. Antennas Propag.*, 2010, **4**, (10), pp. 1543–1548
4 Dobkin, D.M., Weigand, S.M., Iye, N.: 'Segmented magnetic antennas for near-field UHF RFID', *Microw.J.*, 2007, **50**, (6), pp. 872–873
5 Qing, X., Goh, C.K., Chen, Z.N.: 'A broadband UHF near-field RFID antenna', *IEEE Trans. Antennas Propag.*, 2010, **58**, (12), pp. 3829–3838
6 Shi, J., Qing, X., Chen, Z.N., *et al.*: 'Electrically large dual-loop antenna for UHF near-field RFID reader', *IEEE Trans. Antennas Propag.*, 2013, **61**, (3), pp. 1019–1025
7 Wei, X.D., Hu, B.J., Zhang, H.L.: 'Novel UHF near-field RFID reader antenna based on double-sided parallel-strip line', *IEEE Antennas Wirel. Propag. Lett.*, 2014, **13**, pp. 419–422
8 Ding, X.M., Zhang, K., Yu, H., *et al.*: 'A novel magnetic coupling UHF near field RFID reader antenna based on multilayer-printed-dipoles array', *IEEE Trans. Magn.*, 2014, **50**, (1)
9 Li, X., Yang, Z.: 'Dual-printed-dipoles reader antenna for UHF near-field RFID applications', *IEEE Antennas Propag. Lett.*, 2011, **10**, pp. 239–242
10 Ding, X., Wu, Q., Zhang, K., *et al.*: 'A magnetic coupling dipole for UHF near-field RFID reader', *IEEE Trans. Magn.*, 2012, **48**, (11), pp. 4305–4308
11 Cho, C., Lee, C., Ryoo, J., *et al.*: 'Planar near-field RFID reader antenna for item-level tagging', *IEEE Antennas Wirel. Propag. Lett.*, 2011, **10**, pp. 1100–1103
12 Balanis, C.A.: 'Antenna theory: analysis and design' (Harper and Row, 1982)
13 Shen, L., Tang, W., Xiang, H., *et al.*: 'A novel antenna achieving null-less magnetic field distribution for near-field UHF RFID'. Proc. 2014 Int. Symp. on Antennas and Propagation, Kaohsiung, Taiwan, 2014, pp. 547–548